Pergamon

Int. J. Heat Mass Transfer. Vol. 39, No. 9, pp. 1963–1978, 1996

0017-9310/96 $15.00+0.00

0017-9310(95)00253-6

Laminar flow and forced convection heat transfer in plate-type monolith structures by a finite element solution

RAOUL GIUDICI and ENRICO TRONCONI†

Dipartimento di Chimica Industriale e Ingegneria Chimica "G. Natta" del Politecnico, Piazza Leonardo da Vinci 32, I-20133 Milano, Italy

(*Received* 6 *May* 1994 *and in final form* 6 *June* 1995)

Abstract—A numerical solution is obtained by the finite element method for the Graetz problem of forced convection heat transfer in the channels of plate-type monolith catalysts. For this purpose a generalized model is constructed for the duct geometry, the fully developed laminar velocity profile is calculated, and the heat transfer problem is solved for both uniform wall heat flux or temperature. The results are summarized in interpolated functional forms providing the axial evolution of the Nusselt number. Such formulae represent a prerequisite to the development of design equations for mass-transfer coefficients in plate-type monolith catalysts for the selective catalytic reduction of NO_x with ammonia.

INTRODUCTION

Forced convection with laminar flow in straight ducts of a constant cross-section has important practical applications. Shah and London [1] have extensively surveyed the well known Graetz problem for different geometries: from circular ducts to parallel plates, from rectangular sections to triangle passages they attempted to systematize thermal boundary conditions, considering those most common in the literature and interesting in applications. They also reported solutions for sine ducts, elliptical forms, circular sectors and other singly connected configurations, that is geometrical shapes delimited by a single closed line. Double and multiple connected ducts were considered, too.

After Shah and London's publication, other authors have addressed the Graetz problem: different numerical methods have been tested on traditional shapes [2–11]; the less conventional geometries have been studied with regard to entrance effects [12–21]; axial conduction has been considered [22–24]; and finally the analysis of non-Newtonian fluids has begun to appear [25–28].

In this article we consider the forced convection heat transfer problem for ducts of complex geometry corresponding to the channels of plate-type monolith catalysts [29, 30]. We first examine the hydrodynamic problem to obtain information on the laminar velocity profiles inside the monolith channels; then we analyze the heat transfer problem, and eventually derive interpolated expressions for the axial evolution of the Nusselt number with regard to different boundary conditions.

The novelty of this paper lies in the duct geometry considered, as well as in the algorithm adopted for numerical solution of the problem. The choice of the duct geometry is motivated according to two different arguments. First of all, the cross-sections of plate-type monoliths exhibit a peculiar configuration including two non interacting channels. In this paper we illustrate an approach suitable to reduce such a situation to the analysis of a single duct. The same analysis is also expected to provide applied benefits, since catalytic monoliths in plate form are actually of commercial interest for the selective catalytic reduction (SCR) of NO_x with ammonia, SCR processes being the most efficient technology available for the denitrification of flue gases from power stations [30]. It has been shown in the literature [31] that gas–solid mass transfer coefficients in monolithic honeycomb SCR reactors with simple channel geometry (circular, square and triangular) are adequately predicted by relying on the similarity with the corresponding heat transfer problems for constant wall temperature or constant heat flux. It is of practical relevance for the modelling of industrial SCR monolith reactors to establish whether the same conclusions apply also to the class of plate-type monolith catalysts: as mentioned above, however, solutions of the thermal problem for this more complex geometry are not available. While the derivation of such solutions on a generalized basis is the scope of the present work, in a future article [32] they will be applied to the specific purpose of developing a design procedure for plate-type monolithic SCR reactors.

† Author to whom correspondence should be addressed.

NOMENCLATURE

A_H, B_H, C_H, D_H interpolation parameters for $Nu(H2)$—equations (26)–(30)
A_T, B_T, C_T, D_T interpolation parameters for $Nu(T)$—equations (17)–(22)
c_p fluid specific heat
D_h hydraulic diameter
DR geometrical parameter representative of cross sectional shape, $=(R-R_0)$
h heat transfer coefficient
H channel pitch
H' $= 2H$, see Fig. 1
k fluid thermal conductivity
L longitudinal extension of cross section
L_1 $= 4.2335\ H$ see Fig. 1
L_2 $= L-3.173\ H$, see Fig. 1
Nu Nusselt number—(hD_h/k)
p pressure
Pe Peclét number—$(vD_h\rho c_p/k)$
r ratio of dimensionless areas of (B) and (A) sections, respectively—$(S_A D_{hB}^2/S_B D_{hA}^2)$
r_D ratio of hydraulic diameters of (B) and (A) sections, respectively—$(D_{h,A}/D_{h,B})$
r_v ratio of dimensional average velocities of sections B and A, respectively—$(\langle v\rangle_A/\langle v\rangle_B)$
Q volumetric flow rate
R geometrical parameter representative of cross sectional shape—$(L/2H)$
R_0 limiting value of R (= 2.116, see Fig. 1)
S cross-sectional area
T dimensional temperature
T_0 value of the initially uniform temperature profile
$\langle T_{cm}\rangle$ dimensional flow average temperature (cup-mixing)
$\langle T_\Gamma\rangle$ dimensional wall average temperature
v dimensional axial velocity
v^* dimensionless axial velocity—equation (7)
$\langle v\rangle$ dimensional velocity averaged over the duct cross-section
xyz dimensional Cartesian coordinates
$x^*y^*z^*$ dimensionless Cartesian coordinates—equation (7)
z_i^* Graetz axial coordinate $= z/(Pe_i D_{hi})$.

Greek symbols
Γ cross-sectional boundary
μ fluid dynamic viscosity
Θ^* dimensionless temperature—equations (4), (5)
$\langle\Theta_{cm}^*\rangle$ dimensionless flow average temperature (cup-mixing)
$\langle\Theta_\Gamma^*\rangle$ dimensionless wall average temperature
ρ fluid density
τ dimensional peripheral flux
$\langle\tau\rangle$ dimensional peripheral average flux
τ^* dimensionless peripheral flux
ϕ characteristic angle of the cross section (= 57°, see Fig. 1).

Superscripts
$*$ dimensionless variable
∞ asymptotic value for $z \to \infty$.

Subscripts
A relative to (A) geometry—Fig. 1
AB relative to (A) + (B) geometry, i.e. to elementary monolith cells—Fig. 1
B relative to (B) geometry—Fig. 1
cm cup-mixing average
H2 relative to ($H2$)-condition
T relative to (T)-condition
Γ calculated at the duct wall.

Concerning the numerical solution of the partial differential equations associated with either the hydrodynamic or the thermal problem, in this work we adopt the Galerkin finite element method (FEM) rather than more usual approaches based on finite differences or orthogonal collocations. Indeed, the finite element analysis offers some advantages over other methods. Primarily, it gives powerful tools, namely irregular meshes, isoparametric elements [33] and graphical gridding, to reproduce complex geometries such as those involved in the present work; also, FEM provides local and global error estimates useful in adaptive refinement processes and convergence studies [34–36].

THEORY AND METHODS

Geometrical analysis

For our purposes it is first necessary to identify the geometrical domain of interest. In the following, a geometrical reference model is presented.

Inspection of commercial monolith plate-type catalyst matrices shows the existence of an elementary cell in the monolithic section. As represented in Fig. 1, the

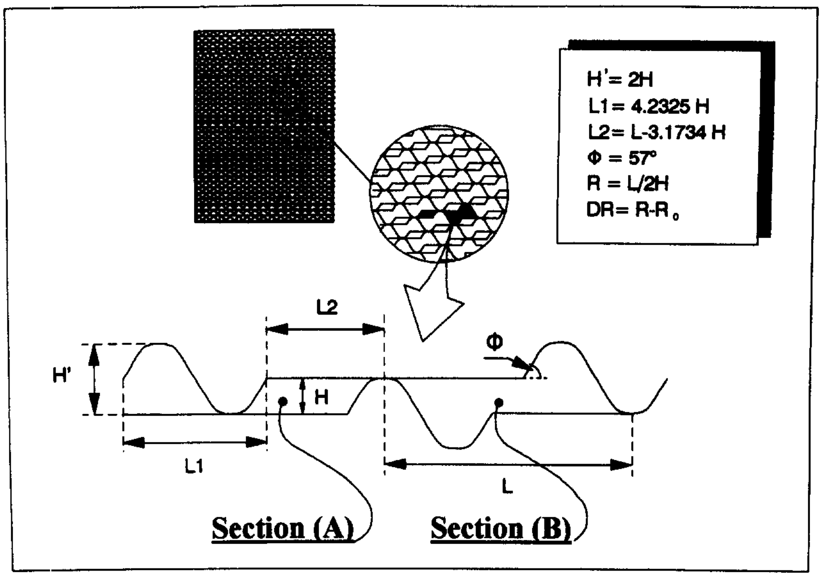

Fig. 1. Typical configuration of plate-type monolith catalyst and two-channel parametric geometrical model. All lengths are in cm.

modular monolith matrix includes two different kinds of geometries which are alternated side by side: the elementary cell consists of a section A, similar to a parallelogram, and a section B, which exhibits characteristic sinusoidal appendices serving as spacers. A representative geometrical parameter DR is defined, which equals the difference between the ratio, $R(=L/2H)$ and its limiting value, R_0 $(=2.116)$, corresponding to compenetration of the sinusoidal appendices with the disappearance of Section A (Fig. 1).

Six values of DR have been chosen for the numerical study of fluid dynamics and heat transfer in the forced convection flow in such sections (see the second column of Table 1). The six values are selected to cover the field of possible industrial interest (a representation of such geometries appears in Fig. 2). Though in the following they are studied individually with respect to both the hydrodynamic and the heat transfer problem, it is worth noting that the six configurations actually serve as a discrete representation of the general geometrical model of plate-type monoliths.

Finally, it is necessary to specify that even if under normal operating conditions communication between the channels may be possible, however the absence of every form of interaction is assumed in the following analysis. This hypothesis results in the identification of two different and separated cross-sections A and B with different geometries, each of them requiring a dedicated investigation of fluid dynamics and heat transfer. Thus, for each DR value the analysis of such two domains will be carried out, as well as a subsequent combination of results to arrive at a unitary representation referring to a single pseudo cross-section of the monolith channel.

Table 1. Geometric and fluid dynamic properties of the investigated geometries

Sample	DR	r	r_D	r_v
1	0.779	0.55777	0.68729	0.39702
2	1.837	0.63827	0.75701	0.51689
3	3.689	0.72034	0.84897	0.63244
4	5.532	0.80671	0.88427	0.69588
5	7.052	0.81096	0.90461	0.75363
6	11.628	0.87216	0.93667	0.85396

The velocity problem

We consider steady-state flow of a fluid with a fully developed laminar velocity profile. Assuming constant physical properties ρ, μ for the fluid and neglecting body forces, centrifugal effects, Coriolis action and electromagnetic interaction, the momentum equation can be written in the following dimensional form [1]:

$$\nabla^2 v = \frac{\partial^2 v}{\partial x^2} + \frac{\partial^2 v}{\partial y^2} = \frac{1}{\mu}\frac{\mathrm{d}p}{\mu\,\mathrm{d}z} = c_1, \tag{1}$$

where v is the axial component of velocity which must satisfy the boundary condition at the border

$$v \equiv 0 \quad \forall\,(x,y) \in \Gamma. \tag{2}$$

We do not take advantage of the oblique symmetry of geometries to avoid the presence of mixed derivatives in equation (1). So we solve the velocity problem in the form of equations (1) and (2), identifying the mathematical boundary Γ with the real channel walls of the monolith. Then we choose a dimensional formulation to impose the same pressure gradients in

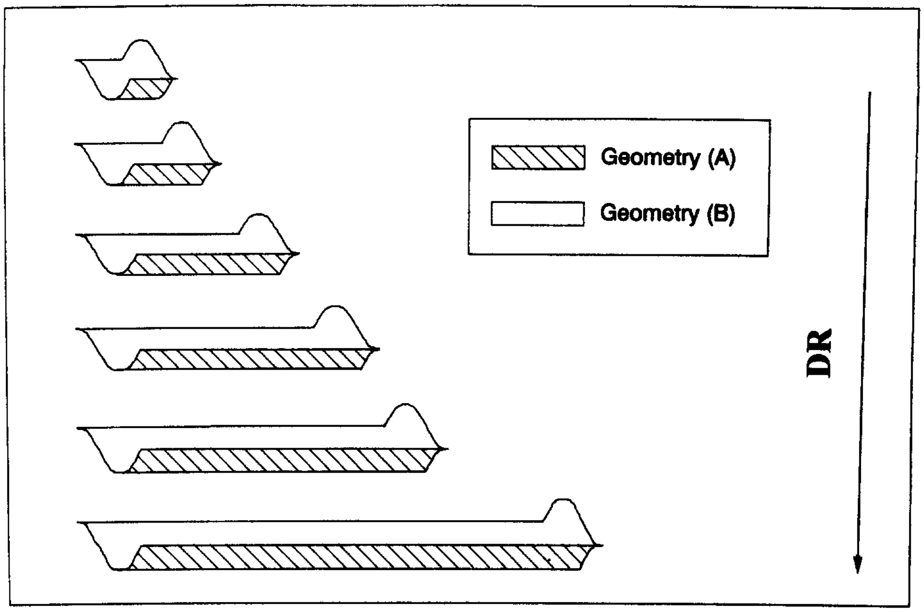

Fig. 2. Elementary cell of the assumed plate-type monolith geometry. *DR* increases from top to bottom.

channels A and B, and we assume the constant c_1 is equal to unity.

Notably, the assumption of laminar flow is consistent with the flow conditions prevailing in SCR monolith catalysts.

The temperature problem

This problem concerns the solution of the energy conservation equation for a fluid in laminar flow in a duct under different thermal boundary conditions [1]. The fluid properties ρ, k, c_p are assumed constant and the laminar fully developed velocity profile is known by assumption, as determined from solution of the hydrodynamic problem. Viscous effects and axial thermal diffusion are neglected and we exclude phase transitions and chemical energy changes. Accordingly, the governing equation is [1]

$$v\rho c_p \frac{\partial T}{\partial z} = k\left(\frac{\partial^2 T}{\partial x^2} + \frac{\partial^2 T}{\partial y^2}\right) \tag{3}$$

with the temperature, T, being the only unknown.

Three different boundary conditions are most often considered [1]: the (T)-condition involves a uniform and constant temperature profile at the wall, both peripherally and axially; the ($H2$)-condition requires a uniformly distributed heat flux on the channel section and a constant average heat flow in the axial direction; the ($H1$)-condition imposes a uniform wall temperature at any cross-section and a constant wall heat transfer rate in the axial direction. In view of the eventual application of the present results to modelling of SCR reactors, in this paper only the (T) and ($H2$) conditions are examined. In fact, they exhibit the same mathematical formulation of the analogous problem concerning gas–solid mass transfer in the monolith channels in the two limiting cases of infinitely fast kinetics (purely physical regime) and infinitely slow kinetics (purely chemical regime), respectively [37–39]. Accordingly, the Nusselt numbers derived from solutions of the two thermal problems provide also the limiting values of the dimensionless gas–solid mass transfer coefficients (Sherwood numbers) for fast and slow kinetics, respectively [31]. This point will be further developed in a forthcoming paper [32].

Referring to the (T) and ($H2$) conditions, the following dimensionless temperatures are usually introduced [1]:

$$\Theta^* = \frac{T - \langle T_\Gamma \rangle}{T_0 - \langle T_\Gamma \rangle} \quad \text{for } (T)\text{-condition} \tag{4}$$

$$\Theta^* = \frac{T - T_0}{\dfrac{\tau D_h}{k}} \quad \text{for } (H2)\text{-condition.} \tag{5}$$

Thus, equation (3) can be rewritten in dimensionless form as

$$v^* \frac{\partial \Theta^*}{\partial z^*} = \frac{\partial^2 \Theta^*}{\partial x^{*2}} + \frac{\partial^2 \Theta^*}{\partial y^{*2}}, \tag{6}$$

where

$$x^* = \frac{x}{D_h} \quad y^* = \frac{y}{D_h} \quad z^* = \frac{z}{PeD_h} \quad v^* = \frac{v}{\langle v \rangle}. \tag{7}$$

Finally, in both situations the initial condition involves a uniform thermal profile, at the value of unity for the (T) case and zero for the ($H2$) case. Then we have

$$(T)\text{-condition}\begin{cases}\text{B.C.} & \Theta^* = 0 \;\; \forall (x^*, y^*, z^*) \in \Gamma \\ \text{I.C} & \Theta_0^* = 1 \;\; \forall (x^*, y^*) \;\; \text{at}\, z^* = 0.\end{cases} \tag{8}$$

$$(H2)\text{-condition}\begin{cases}\text{B.C.} & \tau^* = 1 \;\; \forall (x^*, y^*, z^*) \in \Gamma \\ \text{I.C.} & \Theta_0^* = 0 \;\; \forall (x^*, y^*) \;\; \text{at}\, z^* = 0.\end{cases} \tag{9}$$

Problem analysis

The study of fluid dynamics and heat transfer in the geometrical model of the plate structure is developed along four stages:

(1) Solution of the hydrodynamic problem, equations (1) and (2); since the monolith configuration includes two different kinds of channel sections, the velocity problem has to be solved separately for domains A and B. The operation is repeated for the six different values of the parameter DR.

(2) Definition of a single representative fluid dynamic variable: the construction of a global average velocity ($\langle v \rangle_{AB}$) is proposed. The operation involves the combination of the average velocities in channels A and B ($\langle v \rangle_A$, $\langle v \rangle_B$) for the six different values of DR and the subsequent definition of the relation between $\langle v \rangle_{AB}$ and DR. This results in the construction of a functional from $\langle v \rangle_{AB}(DR)$ which allows a global one-dimensional representation of fluid dynamics for every value of DR. Construction of $\langle v \rangle_{AB}$ is described in the Results and Discussion Section.

(3) Solution of the temperature problem, equations (3) and (4) (T-condition) or equations (3)–(5) ($H2$-condition), and determination of the streamwise evolution of the Nusselt number along the axial coordinate. As in point 2 above, the study of two different Sections A and B is required for six different values of DR, so that 12 discrete axial profiles of the Nusselt number are generated.

(4) Definition of a single representative heat transfer variable: like in the velocity problem the construction of a single Nusselt number (Nu_{AB}) is proposed for the six geometries to represent the heat transfer process in a global way. The operation is organized in three subsequent steps:

(a) combination of channel A and B Nusselt numbers (Nu_A, Nu_B) and definition of a global Nusselt number (Nu_{AB})

$$Nu_{AB} = \frac{D_{hAB} h_{AB}}{k} = \frac{D_{hAB} \langle \tau \rangle_{AB}}{k(\langle T_{cm} \rangle_{AB} - \langle T_T \rangle_{AB})}. \tag{10}$$

The calculations are made using the discrete axial profiles of Nu_A and Nu_B constructed by numerical solution of the temperature problem and yields six discrete values of global $Nu_{T,AB}$ as well as six values of global $Nu_{H2,AB}$ along z^*_{AB} the global axial coordinate.

(b) Empirical fitting of the relationship between Nu_{AB} and z^*_{AB}. This operation is carried out for every chosen value of DR, and leads to the definition of six global $Nu_{T,AB}$ and six global $Nu_{H2,AB}$ continuously defined along z^*_{AB}.

(c) Identification of analytical models representative of the heat transfer characteristics of all the considered geometries, reproducing in a continuous fashion the relationship between the axial evolution of the global Nusselt number and the parameter DR: the results obtained from FEM simulations are extended to the whole geometrical model and a generalized functional form $Nu_{AB}(z^*_{AB}, DR)$ is derived for both (T) and ($H2$) conditions.

Numerical methods

The analysis of the problem requires the solution of partial differential equations as well as the regression of results (in terms of Nusselt numbers) as functions of z^*_{AB} and DR.

Nonlinear regressions are carried out using the FORTRAN program BURENL [40], implementing a collection of direct and indirect search methods for minimization of the residual sum of squares.

For the solution of PDEs, an adequate numerical approach must be implemented in order to meet satisfactorily the boundary conditions associated with the complex duct geometry. In this work we apply the Galerkin finite element method [33].

The basic idea of FEM consists in reducing the problem size by dividing the domain into smaller regions, called elements, where the governing equations are approximated according to the methods of weighted residuals. Within each element the simplified governing equations have the same formal expression, and can be assembled to retain the unity of the problem and the continuity of the solution to generate an overall system of algebraic or ordinary differential equations, depending on the nature of the original PDEs. Since the element is an independent unit, it can be locally adjusted to describe a particular boundary: this secures a higher accuracy for the description of complex domains than offered by, e.g. finite differences of orthogonal collocations.

In order to allow an easy description of the geometrical model of Fig 1, isoparametric serendipity second-order elements (triangular-six nodes and quadrilateral-nine nodes) [33] and graphical gridding have also been implemented in a specific FORTRAN code. Also, solution of the overall system of equations has been carried out by Gaussian elimination (for axial-developed problems) and by Gear's multivalue ODE integration method [41] (for axially developing problems), achieving efficient convergence. Finally, an accurate phase of postprocessing produces graphical tools to check the results qualitatively and quantitatively.

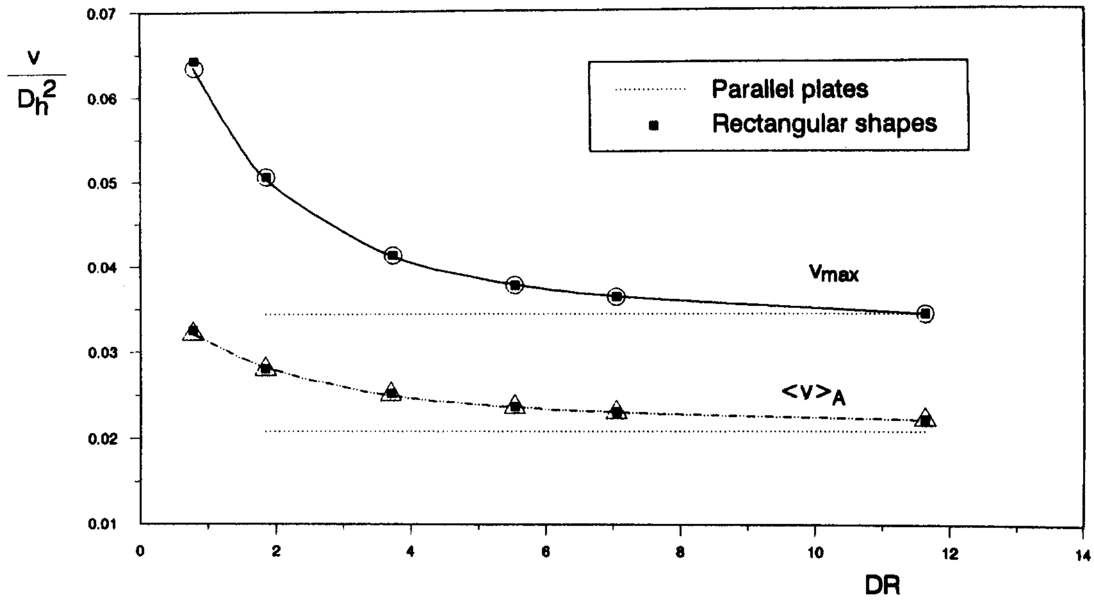

Fig. 3. Velocity problem: maximum and average velocity for channels A vs DR. The velocities are divided by the squared hydraulic diameter so as to be compared with rectangular shape and parallel plate literature data [1]. All results are relative to a unit c_1 constant [see equation (1)].

RESULTS AND DISCUSSION

The velocity problem

Section (A). The study of channel A reveals a similarity with the hydrodynamics of laminar flow in rectangular ducts. Indeed, large aspect ratios make the influence of the oblique sides negligible, so that a parabolic velocity profile covers most of each section, giving average and maximum velocities close to the corresponding literature data [1] for rectangular channel shapes (Fig. 3). In the limit of $DR \to \infty$ the situation of parallel plates is recovered.

Section (B). The analysis of laminar flow in channels B shows a different and more complex situation, as illustrated in Fig. 4. For large values of DR the velocity profile includes two different contributions: on one hand the curvilinear appendices exhibit a typical concentric sinusoidal profile; on the other hand the central portion shows an approximately parabolic profile quite similar to the case of long rectangles or parallel plates. For small values of DR the two contributions compenetrate each other and it becomes impossible to trace their distinctive features separately.

A synthetic representation of average and maximum velocities upon varying DR is shown in Fig. 5: even if increasing DR reduces the average velocity, the maximum velocity does not converge to that characteristic of parallel plates. Thus, differently from Sections A, the parallel plates provide an asymptotic situation for B geometries only in a mean sense.

Combination. In order to achieve a unitary representation of fluid dynamics for the two-channel model of Fig. 1 we define a global average velocity ($\langle v \rangle_{AB}$). For each considered value of DR it is calculated according to the following equation:

$$\langle v \rangle_{AB} = \frac{\langle v \rangle_A S_A + \langle v \rangle_B S_B}{S_A + S_B}. \tag{11}$$

The volumetric flow rate (Q) is treated in the same way, too.

To generalize the results, both $\langle v \rangle_{AB}$ and Q are then expressed as functions of the geometrical parameter DR. The resulting empirical formulas are shown below [equations (12) and (13)]

$$\langle v \rangle_{AB} = 0.0154 + 9.78 \times 10^{-3} DR^{-2.44 \times 10^{-1}} \times \exp(-1.48 \times 10^{-1} DR) \tag{12}$$

$$Q_{AB} = 4.986 \times 10^{-2} + 1.035 \times 10^{-2} DR. \tag{13}$$

Both equations yield less than 0.3% errors when compared to calculated data.

The temperature problem

In the following, the (T) and $(H2)$ boundary conditions will be treated separately for the sake of clarity.

(T)-Condition

Section (A). For channel A the use of about 300 nodes and nonuniform meshes leads to converged results in accordance with literature data [1] for rectangular duct shapes, which confirms the negligible contribution of oblique sides. The results plotted in Fig. 6 show that increasing DR brings about greater

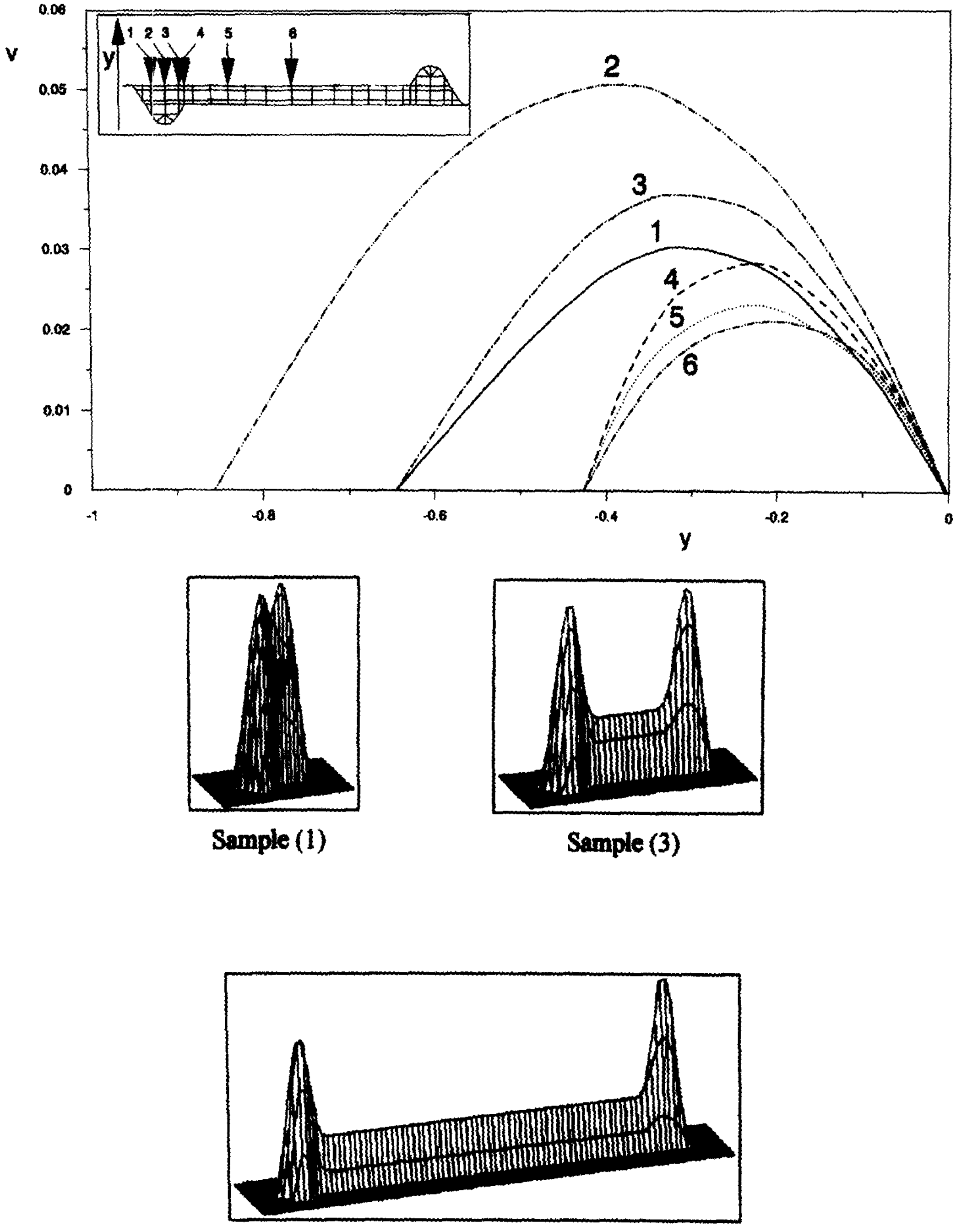

Fig. 4. Velocity problem: fully developed laminar velocity profiles in channels B.

Nusselt numbers: in the limit of $DR \to \infty$ the same Nu evolution as in parallel plates is recovered.

Section (*B*). The study of Section B reveals a more complex situation dominated by two different asymptotic behaviours (see Fig. 7):

(1) In the entrance region (see Table 2 and Fig. 8) the smaller thermal resistance of the parallel sides in section B prevails on the longer effective conduction path length for energy transfer from wall to bulk associated with the corner-shaped sinusoids, so that heat transfer is controlled by the central portion of Section B, and a thermal behavior similar to that of ducts with rectangular cross-sections is evident. Also, increasing DR emphasizes the importance of the central zone, resulting in a reduced average heat transfer resistance. Thus, like for Section A, at small z_B^* increasing DR results in greater Nusselt numbers: in the limit

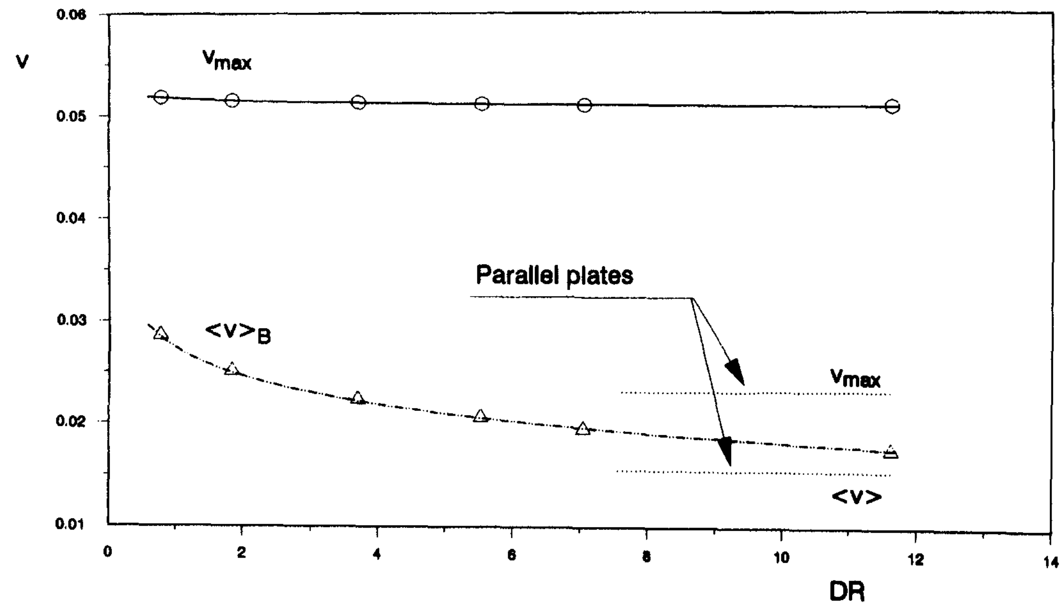

Fig. 5. Velocity problem: maximum and average velocity for channels B vs DR. All results are relative to a unit c_1 constant [see equation (1)].

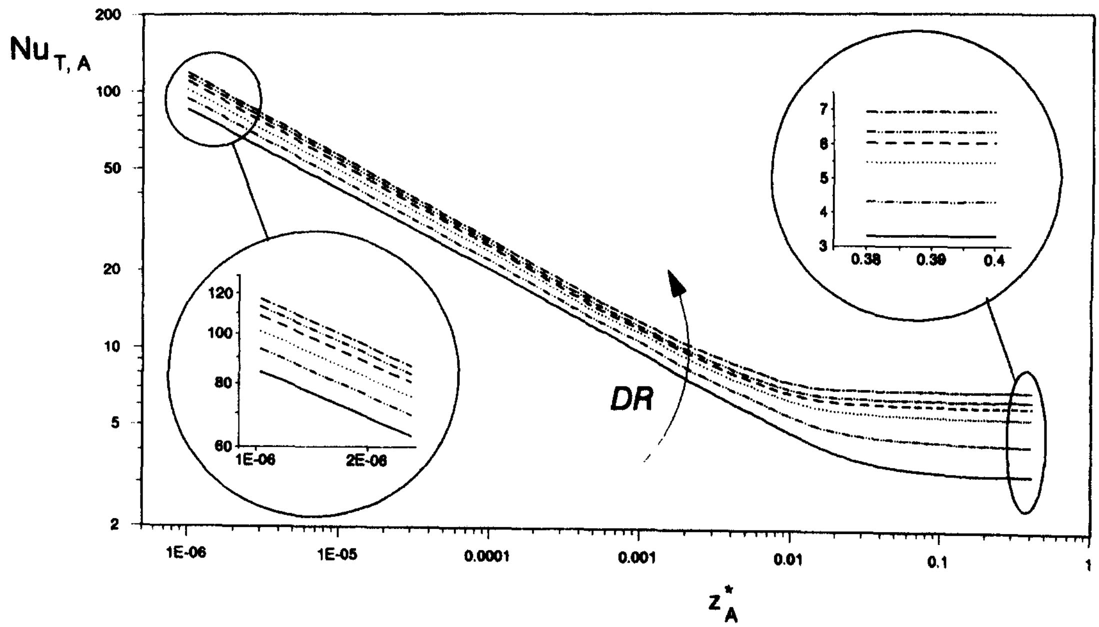

Fig. 6. (T)-condition: axial evolution of the Nusselt number of channels A.

of $DR \to \infty$, the Nu-evolution typical of parallel plates is recovered. In fact, for the sixth geometry ($DR = 11.628$) at $z_B^* = 1.0 \times 10^{-6}$ we calculate $Nu = 118.19$, which is close to literature data [1] for parallel plates (122.94).

(2) On the other hand, in the region of nearly developed thermal profile the Nusselt number of Section B is controlled by the curved appendices (see Table 2 and Fig. 8). Because of its smaller thermal resistance, in fact, the central zone is reached before thermal equilibrium with the wall, so that its contribution to heat transfer becomes already negligible when the T-profiles in the sinusoids are still evolving. Under such conditions an increment of DR produces two opposite effects: while it enhances heat transport in the central region, it also causes the same central portion to reach earlier thermal equilibrium with the wall, which makes the sinusoidal appendices con-

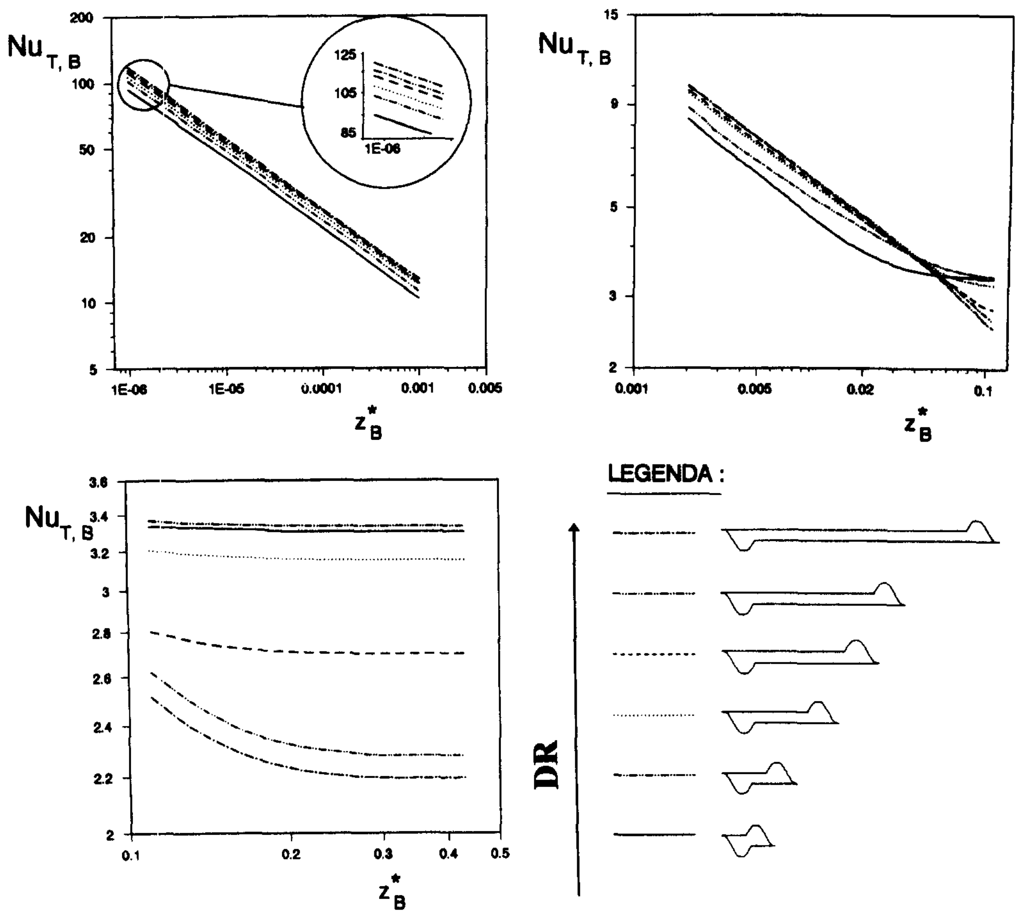

Fig. 7. (T)-condition: axial evolution of the Nusselt number for channels B. For the sake of clarity the representation is subdivided into three different portions showing the rectangle-like and sine-like asymptotic behaviours and the intermediate transition.

trolling the wall—bulk heat transfer process over a longer stretch of the axial coordinate. For small DR the first effect is stronger; for larger sections the second one dominates: this explains the dependence of the asymptotic Nusselt number on DR characterized by an inflection point shown in Figure 9. Notice that, in contrast with the situation of the entrance region, here for $DR \to \infty$ one approaches asymptotically the heat transfer behaviour of the sinusoidal section: our numerical solution yields $Nu_B^{\infty} = 2.195$ (confirmed by an additional test for $DR = 15$), which is close to the literature data of 2.12 for sinusoidal ducts [1]; the small difference is due to an interaction with the central region which cuts off at three quarters the sinusoids and slightly enhances the heat transfer efficiency. The weak maximum of Nu_B^{∞} in the region of small DR in Fig. 9 can be rationalized by the transition to a completely different fluid dynamic situation devoid of the central parabolic contribution and exclusively dominated by the sinusoidal appendices.

Combination. In order to achieve a unique Nusselt number of a one-dimensional representation, a global $Nu_{T,AB}$ is calculated, using the discrete axial profiles of $Nu_{T,A}$ and $Nu_{T,B}$ generated by numerical solution of the temperature problem. The formulae employed for this purpose involve the fluid dynamic hypothesis of equal pressure loss in the channels. They make use of the dimensionless relationships (4), (5) and (7) and of the Nusselt number definition [equation (10)]: on this subject notice that Sections A and B have different hydraulic diameters D_h and that the construction of $Nu_{T,AB}$ requires the use of a combined hydraulic diameter ($D_{h,AB}$). Finally the formulae consider the phase displacement between the Graetz-coordinates of the channels (z_A^* and z_B^*) and that of the elementary cell (z_{AB}^*)

$$z_A^* = \frac{z}{Pe_A D_{hA}} = z_{AB}^* \frac{(1+r_D^2 r)(1+r_v r_D^2 r)}{r_v r_D^2 (1+r_D r)^2} \tag{14}$$

$$z_B^* = \frac{z}{Pe_B D_{hB}} = z_{AB}^* \frac{(1+r_D^2 r)(1+r_v r_D^2 r)}{(1+r_D r)^2}, \tag{15}$$

where r_D equals the ratio of hydraulic diameters ($D_{h,A}/D_{h,B}$); r_v compares the dimensional average velocities ($\langle v \rangle_A / \langle v \rangle_B$); and r represents the proportion between dimensionless areas ($S_A D_{hB}^2 / S_B D_{hA}^2$); for

Table 2. Entrance and asymptotic Nusselt numbers for the (*T*)-condition in channel B

z_B^*	Sample (1)	Sample (2)	Sample (3)	Sample (4)	Sample (5)	Sample (6)
0.10×10^{-6}	0.93461×10^{2}	0.10170×10^{3}	0.10645×10^{3}	0.11137×10^{3}	0.11450×10^{3}	0.11820×10^{3}
∞	0.33081×10^{1}	0.33400×10^{1}	0.31550×10^{1}	0.26990×10^{1}	0.22810×10^{1}	0.21950×10^{1}

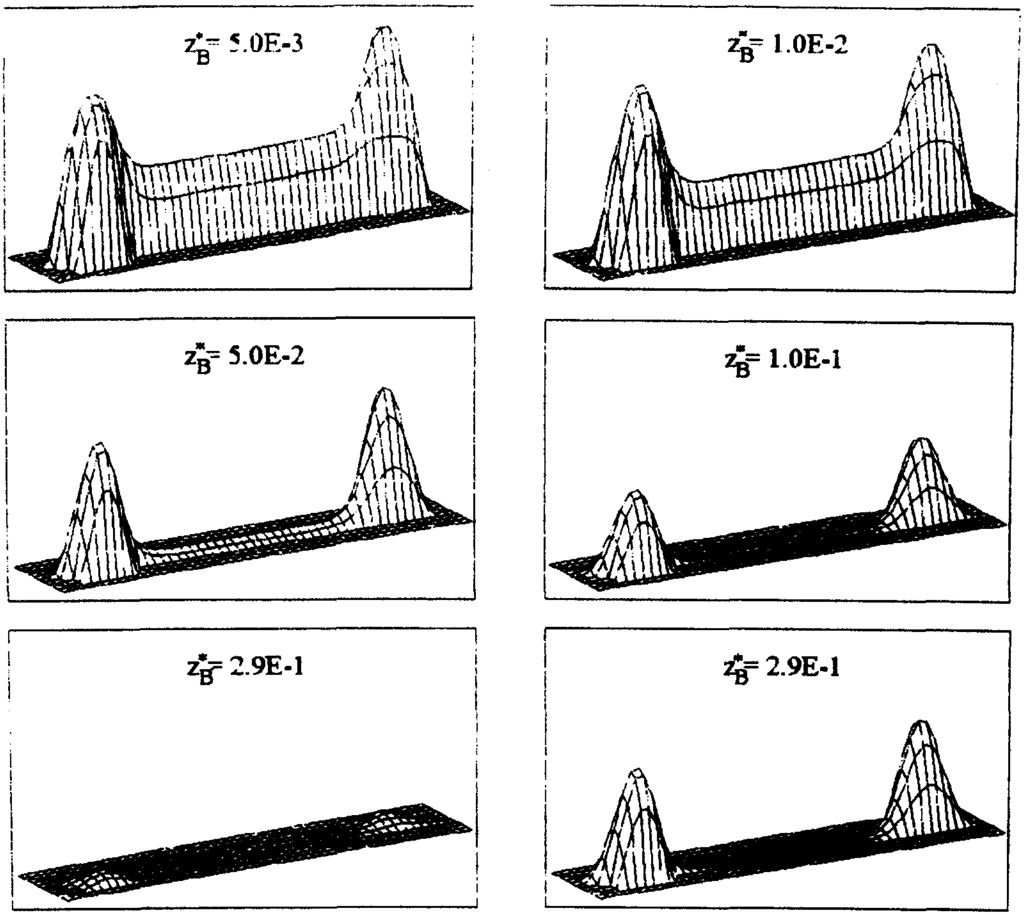

Fig. 8. (*T*)-condition, sample 4, channel B: temperature distribution over the cross-section at different values of the axial coordinate.

numerical values of these parameters see the last columns of Table 1.

So for the (T)-condition we have

$$Nu_{\mathrm{T,Ab}} = \frac{(1+r_D^2 r)}{(1+r_D r)} \frac{\langle\Theta_{cm}^*\rangle_B Nu_B + \langle\Theta_{cm}^*\rangle_A Nu_A r}{\left(\dfrac{\langle\Theta_{cm}^*\rangle_B + \langle\Theta_{cm}^*\rangle_A r_v r_D^2 r}{1+r_v r_D^2 r}\right)}. \tag{16}$$

The calculation, made for every chosen value of DR, produces the axial profiles shown in Fig. 10. Here, the calculated results are represented by triangular symbols, whereas, a solid line shows the interpolating model based on the following functional form:

$$Nu_{\mathrm{T,AB}} = Nu_{\mathrm{T,AB}}^{\infty} + A_T(1000 z_{AB}^*)^{-B_T}$$
$$\times \frac{\exp(-C_T(D_T+z_{AB}^*))}{\exp(-C_T(D_T+z_{AB}^*))+\exp(C_T(D_T+z_{AB}^*))}. \tag{17}$$

The form of equation (17) derives both from empirical consideration and from usual literature expressions [42]. Among the tested models, it best reproduces the characteristic shape due to the presence of two different asymptotic Nusselt numbers (Nu_A^{∞} and Nu_B^{∞}): it secures less than 0.5% errors for all the six values of *DR*.

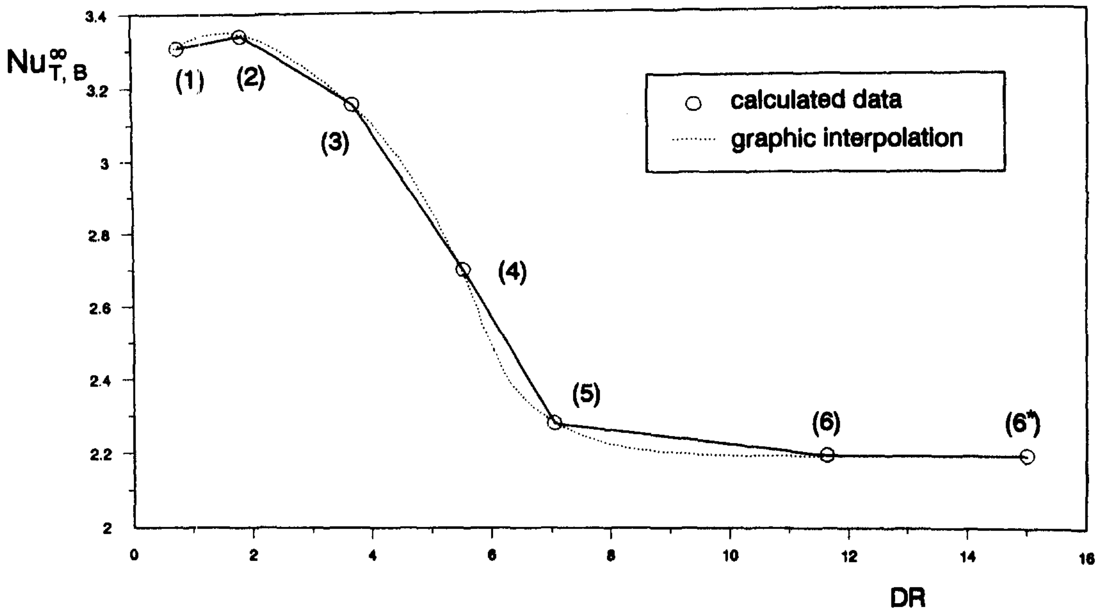

Fig. 9. (T)-condition: asymptotic Nusselt number in channels B vs DR. In addition to the values calculated for the six samples of Table 1 the asymptotic number of $DR = 15$ is reported to confirm the trend for $DR \to \infty$.

To extend the results to all the other possible configurations of the geometrical model, the calculated values of A_T, B_T, C_T, D_T and the combined $Nu^{\infty}_{T,AB}$ are fitted as functions of DR. The results of this analysis are summarized in the following:

$$A_T(DR) = 11.665 + 192.167 DR^{0.2851} \exp(-0.9027 DR) \times \exp(-1.5 DR^2 + 1.267 DR + 8.8671) \quad (18)$$

$$B_T(DR) = 0.3467 + 5.0373 \times 10^{-2} DR^{0.30723} \times \exp(-0.49634 DR) \quad (19)$$

$$C_T(DR) = 10.1252 + 0.9877 \exp(0.1186 DR) \quad (20)$$

$$D_T(DR) = -0.09948 + 3.5016 DR^{0.76301} \times \exp(-2.2214 DR^{0.53113}) \quad (21)$$

$$Nu^{\infty}_{T,AB}(DR) = 2.195 - 0.03524(DR^{4.2495} + 6.9217 DR) \times \exp(-0.7039 DR) \log(0.1899 DR). \quad (22)$$

Notice that all the functional forms above derive from purely empirical considerations: since we are performing a regression on regression results, it is not possible to associate any physical meaning with the parameters values. In terms of accuracy, however, the above formulation seems quite satisfactory: it reproduces the relation $Nu_{T,AB}(DR, z^*_{AB})$, and by means of a simple one-dimensional energy balance integration

$$\frac{d\langle \Theta^*_{cm} \rangle}{dz^*} = -4Nu(\langle \Theta^*_{cm} \rangle - \langle \Theta^*_T \rangle) \quad (23)$$

it gives the axial evolution of the flow average global temperature ($\langle \Theta^*_{cm} \rangle_{AB}$) with less than 5% errors when compared to FEM rigorous but extremely more expensive results.

(H2)-Condition

Section (A). The axial evolution of the calculated Nusselt number upon varying DR are shown in Fig. 11. A section of larger DR gives a bigger Nu_B, although the growth of the Nusselt number is slower than in the (T) case. Similar to that case, however, the behaviour of typical of parallel plates is asymptotically recovered for $DR \to \infty$.

Section (B). For the ($H2$)-condition all numerical studies show a different situation with respect to the (T)-condition (Fig. 12). Indeed, the reason for the distinction is clear: the ($H2$)-condition, involving a constant heat flux, indefinitely allows for heat exchange also in the central block of the channel section. Therefore, the present condition lets the behaviour of parallel plates be the natural asymptote ($DR \to \infty$) for the (B) geometry at every z^*_B.

Combination. The global Nusselt number ($Nu_{H2,AB}$) is calculated according to the following equation:

$$Nu_{H2,AB} = \frac{1}{\dfrac{Nu_B r_D^2 r + Nu_A}{Nu_A Nu_B (1 + r_D^2 r)} = 4 z^*_{AB} \dfrac{r(r_v r_D - 1)^2}{r_v (r r_D + 1)^2}}. \quad (24)$$

Equation (24) derives from a combination process similar to that for the (T)-condition: the parameters r, r_v and r_D have the same meaning (Table 1) and z^*_{AB} still represents the Graetz-coordinate based on a glo-

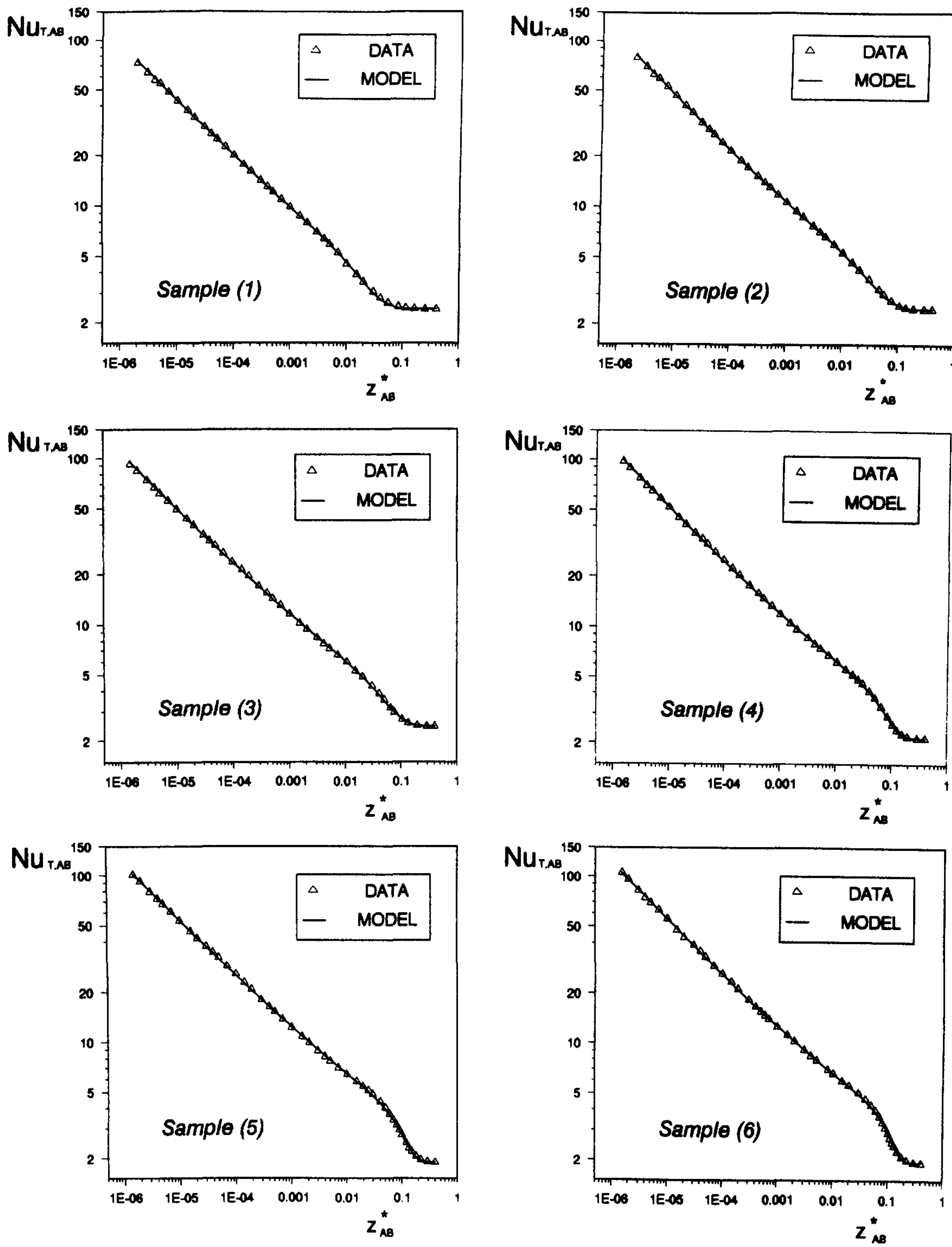

Fig. 10. (T)-condition: axial evolution of the global Nusselt number. Discrete results and interpolating model.

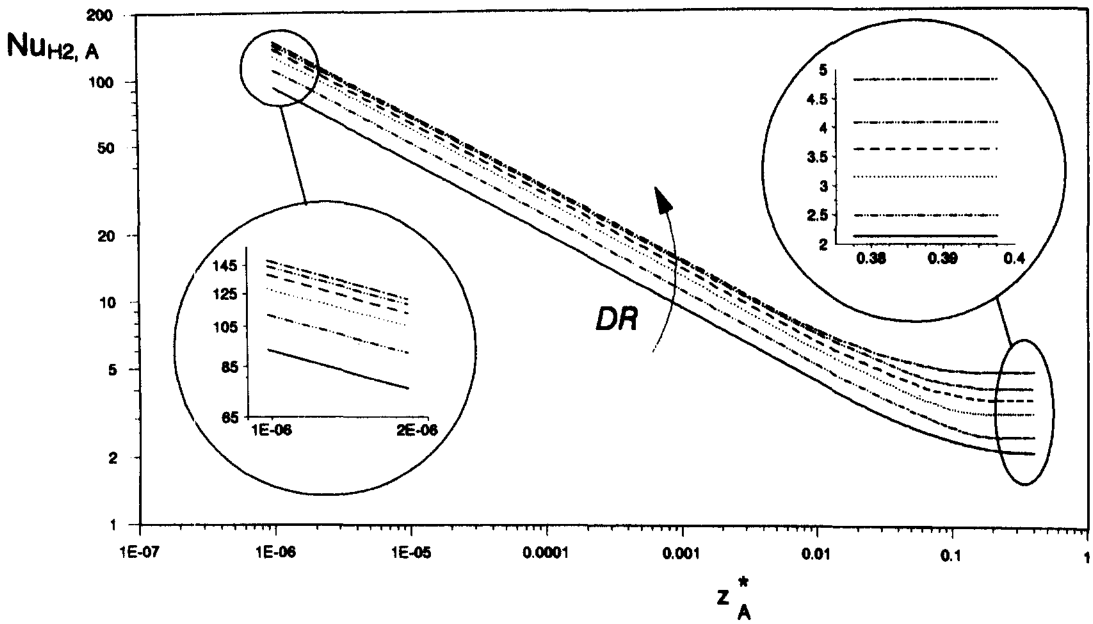

Fig. 11. ($H2$)-condition: axial evolution of Nusselt number in channels A. Legend of the curves as in Fig. 7.

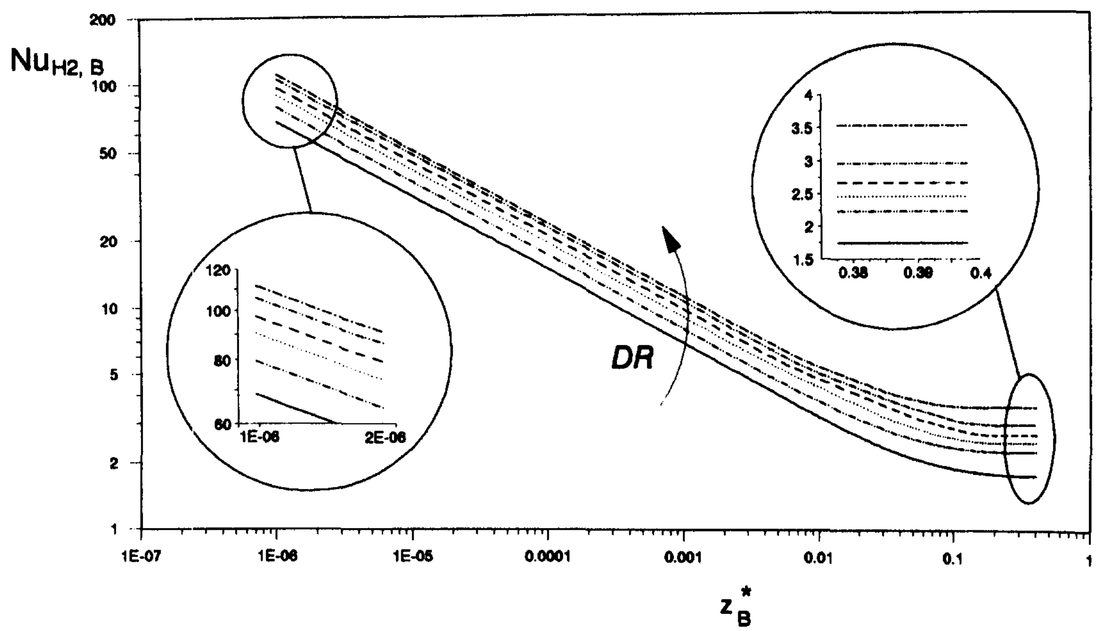

Fig. 12. ($H2$)-condition: axial evolution of Nusselt number in channels B. Legend of the curves as in Fig. 7.

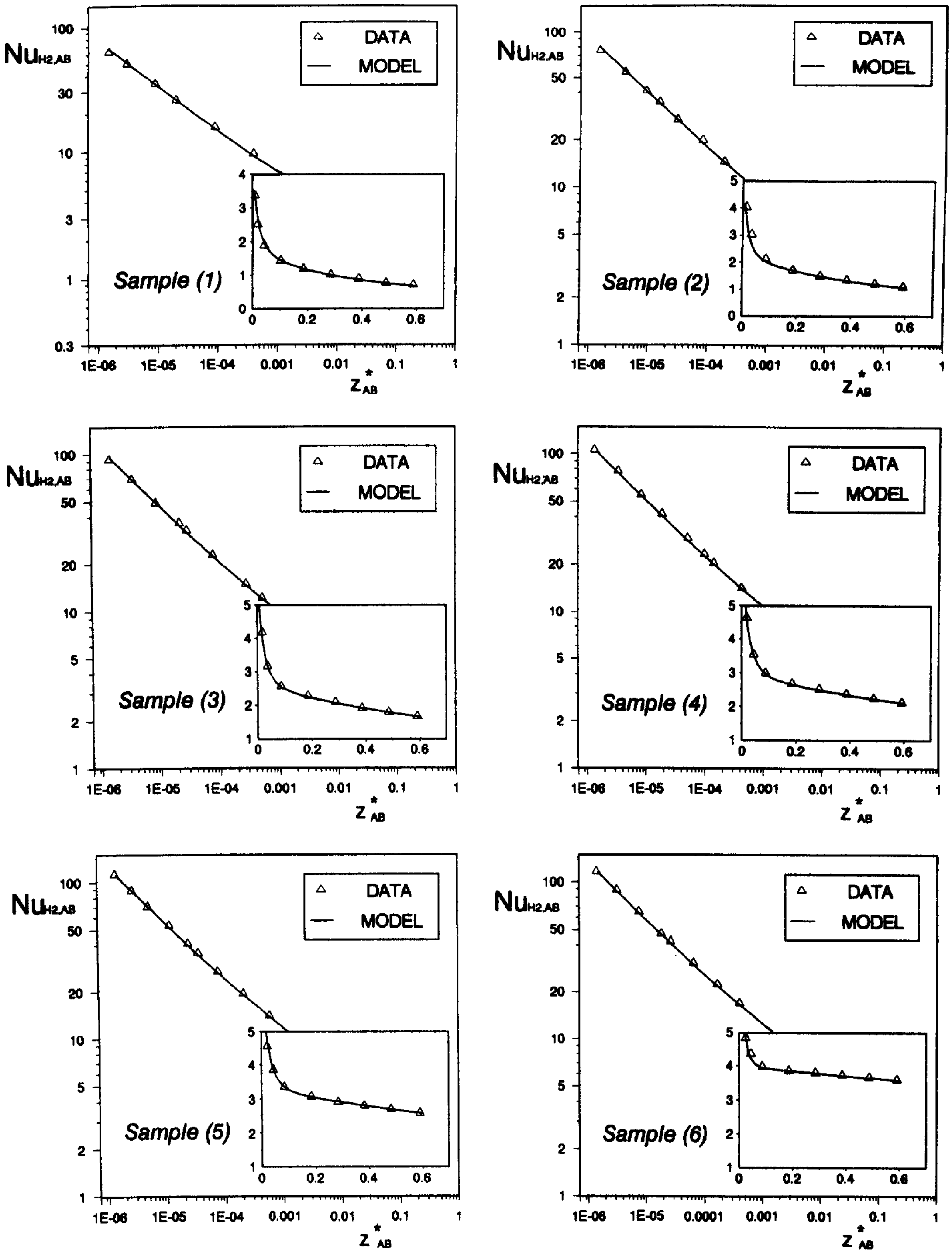

Fig. 13. ($H2$)-condition: axial evolution of global Nusselt number. Discrete results and interpolating model.

bal elementary cell [equations (14) and (15)]. In addition we only introduce in equation (24) the well known axial evolution of the flow average temperatures for the ($H2$) condition ($i = A,B$) [1]

$$\langle \Theta^*_{cm} \rangle_i = 4z^*_i. \tag{25}$$

The discrete axial profiles obtained from this operation are fitted satisfactorily by an equation in the form (see Fig. 13):

$$Nu_{H2,AB} = \frac{1}{A_H + B_H z^*_{AB}} + C_H (1000 z^*_{AB})^{-D_H} \exp(-30 z^*_{AB}). \tag{26}$$

Equation (26) secures less than 1.5% error in calculating the flow average global temperature ($\langle\Theta^*_{cm}\rangle_{AB}$).

Like the (T)-condition, the relationship between global Nusselt number and geometry of the channel section is described by means of parameters A_H, B_H, C_H, D_H, whose values calculated for the six selected DR values are adequately fitted by the following empirical expressions:

$$A_H(DR) = 0.1215+0.4114DR^{0.2451} \times \exp(-0.0477DR) \quad (27)$$

$$B_H(DR) = 1.5727DR^{-0.5550}\exp(-0.1807DR) \quad (28)$$

$$C_H(DR) = 9.2610-4.7589DR^{-0.0121} \times \exp(-0.2717DR) \quad (29)$$

$$D_H(DR) = 0.3889-0.0072DR^{-0.0338} \times \exp(-0.1975DR). \quad (30)$$

Notice that in the limit of $z^*_{AB} \to \infty$ we always have $Nu_{H2,AB}$ approaching zero, except for $DR \to \infty$. This peculiarity is due to the procedure for combination of the results of Sections A and B.

We recommend use of equations (17)–(22) and (26)–(30) only in the tested range of DR values (0.778–11.628).

CONCLUSIONS

A generalized numerical solution of the forced convection heat transfer problem in the channels of plate-type monolith structures has been obtained for constant physical properties of the fluid stream and fully developed laminar flow. The analysis, which also involved the definition of the developed velocity profile, has been carried out using the finite element method (FEM) for numerical solution of the governing partial differential equations. Simulations were made with reference to a generalized two-channel geometric model derived from inspection of commercial plate-type monolith catalysts for SCR-DeNO$_x$ applications.

The results of the hydrodynamic problem have been summarized in a global average velocity profile given as a function of the single geometrical parameter DR.

The temperature problem has been solved both for a constant wall temperature (T-condition) and for a peripherally and axially constant heat flow ($H2$-condition). A global Nusselt number (Nu_{AB}) has been derived in order to describe wall-gas heat transfer in the two-channel duct according to a simple one-dimensional approach. Also, equations have been derived to fit FEM results, representing the dependence of the axial evolution of the global Nusselt number ($Nu_{AB}(z^*_{AB})$) on the cross-sectional shape (i.e. on DR). This has resulted in the definition of design expressions ($Nu_{T,AB}(DR,z^*_{AB})$ and $Nu_{H2,AB}$ (DR,z^*_{AB})), which allow calculation of the axial profile of the global bulk temperature along the monolith ducts by simple integration of the macroscopic one-dimensional energy balance for every configuration of the present geometrical model.

The values of the Nusselt number calculated in this work for the T- and the $H2$-boundary conditions represent asymptotic limits for the dimensionless gas–solid mass transfer coefficients (Sherwood numbers) in plate-type monolith catalysts. Application of the present results to design methods for chemical reactors using plate-type monoliths in the selective catalytic reduction of nitrogen oxides will be reported in a future paper.

REFERENCES

1. R. K. Shah and A. L. London, *Laminar Flow Forced Convection in Ducts*, Supplement 1 to *Advances in Heat Transfer*, Academic Press, New York (1978).
2. T.-M. Shih, A literature survey on numerical heat transfer (1984–1985), *Numer. Heat Transfer* **11**, 1 (1987).
3. G. E. Schneider and M. J. Raw, Control volume finite-element method for heat transfer and fluid flow using colocated variables—1. Computational procedure, *Numer. Heat Transfer* **11**, 363 (1987).
4. G. E. Schneider and M. J. Raw, Control volume finite-element method for heat transfer and fluid flow using colocated variables—1. Application and validation, *Numer. Heat Transfer* **11**, 391 (1987).
5. C. P. Tzanos, Central difference-like approximation for the solution of convection–diffusion problems, *Numer. Heat Transfer B Fundam.* **18**, 97 (1990).
6. A. Rigal, Numerical analysis of three-time-level finite difference schemes for unsteady diffusion–convection problems, *Int. J. Numer. Meth. Engng* **30**, 307 (1990).
7. M. Peric, R. Kessler and G. Scheuerer, Comparison of finite-volume numerical methods with staggered and colocated grids, *Comput. Fluids* **16**, 389 (1988).
8. W. Braga, On the use of some weighted upwind schemes for strongly convective flows, *Numer. Heat Transfer B Fundam.* **18**, 43 (1990).
9. B. Ramaswamy, Efficient finite element method for two-dimensional fluid flow and heat transfer problem, *Numer. Heat Transfer B Fundam.* **17**, 123 (1990).
10. G. D. Thiart, Finite difference scheme for the numerical solution of fluid-flow and heat transfer problem in non-staggered grids, *Numer. Heat Transfer B Fundam.* **17**, 43 (1990).
11. C.-K. Chen, K.-L. Wong and M.-S. Lee, Finite element solution of time-dependent flow and heat transfer characteristics around a circular cylinder, *Comput. Struct.* **33**, 771 (1989).
12. Z. F. Dong and M. A. Ebadian, A numerical analysis of thermally developing flow in elliptic ducts with internal fins, *Int. J. Heat Fluid Flow* **12**, 166 (1991).
13. K. Oyakawa and I. Mabuchi, Fluid flow and heat transfer in a parallel plate duct containing a cylinder, *Bull. JSME* **24**, 1795 (1981).
14. D. E. Metzeger, R. A. Berry and J. P. Bronson, Developing heat transfer in rectangular ducts with staggered arrays of short pin fins, *J. Heat Transfer* **104**, 700 (1982).
15. V. M. Iyevlev, B. V. Dzubenko, G. A. Dreitser and V. V. Balashov, Unsteady-state heat and mass transfer in complex-shaped channels, *Int. J. Heat Mass Transfer* **32**, 1389 (1989).
16. A. C. Trupp and Q. M. Lei, Laminar flow heat transfer in circular sector ducts with uniform heat flux, *Trans. Can. Soc. Mech. Engrs* **13**, 31 (1989).
17. A. C. Trupp and A. C. Y. Lau, Fully developed laminar

heat transfer in circular sector ducts with isothermal walls, *J. Heat Transfer* **106**, 467 (1984).
18. R. M. Manglik and A. E. Bergles, Laminar flow heat transfer in a semi-circular tube with uniform wall temperature, *Int. J. Heat Mass Transfer* **31**, 625 (1988).
19. B. R. Baliga and R. R. Azrak, Laminar fully developed flow and heat transfer in triangular plate-fin ducts, *J. Heat Transfer* **108**, 24 (1986).
20. G. E. Schneider and B. L. LeDain, Fully developed laminar flow and heat transfer in an arbitrarily shaped triangular duct, *Wärme-und Stoffübertr.* **18**, 85 (1984).
21. Y. Asako and M. Faghri, Three-dimensional laminar heat transfer and fluid flow characteristics in the entrance region of a rhombic duct, *J. Heat Transfer* **110**, 885 (1988).
22. H. Brauer, Heat transfer in tubes with laminar flow and axial heat conduction, *Wärme-und Stoffübertr.* **15**, 137 (1981).
23. H. Hagasue, Steady-state heat transfer with axial conduction in laminar flow in a circular tube with a specified temperature or heat flux wall, *Int. J. Heat Mass Transfer* **24**, 1823 (1981).
24. C. Laohakul, C. Y. Chan, K. Y. Look and C. W. Tan, On approximate solutions of the Graetz problem with axial conduction, *Int. J. Heat Mass Transfer* **28**, 541 (1985).
25. B. F. Blackwell, Numerical solution of the Graetz problem for a Bingham plastic in a laminar tube flow with constant wall temperature, *J. Heat Transfer* **107**, 466 (1985).
26. C.-T. Liou and F.-S. Wang, Solutions to the extended Graetz problem for a power-model fluid with viscous dissipation and different entrance boundary conditions, *Numer. Heat Transfer A Applic.* **17**, 91 (1990).
27. I. O. Mohamed, R. G. Morgan and R. Y. Ofoli, Average convective heat transfer coefficients in single screw extrusion of non-Newtonian food materials, *Biotechnol. Prog.* **4**, 68 (1988).
28. R. S. Parikh and R. Mahalingam, Collocation approach to laminar flow heat transfer in non-Newtonian fluids, *Chem. Engng J. Biochem. Engng J.* **38**, 1 (1988).
29. S. Irandoust and B. Andersson, Monolithic catalysts for nonautomobile applications, *Catal. Rev.-Sci. Engng* **30**, 341 (1988).
30. H. Bosch and F. Janssen, Catalytic reduction of nitrogen oxides, *Catal. Today* **2**, 369 (1988).
31. E. Tronconi and P. Forzatti, Adequacy of lumped parameter models for SCR reactors with monolith structure, *AIChE J.* **38**, 201 (1992).
32. R. Giudici, E. Tronconi and P. Forzatti, Design methods for plate-type monolith catalyst used in the selective catalytic reduction of NO_x (in preparation).
33. D. S. Burnett, *Finite Element Analysis. From Concepts to Applications*, Addison Wesley, Reading (1988).
34. B. A. Szabo, Estimation and control of error based on p convergence. In *Accuracy Estimates and Adaptive Refinements in Finite Element Computations* (Edited by I. Babuška, O. C. Zienkiewicz, J. Gago and E. R. de A. Oliveira), pp. 61–79. Wiley, Chichester (1986).
35. R. E. Bank, Analysis of local *a-posteriori* error estimate for elliptic equations. In *Accuracy Estimates and Adaptive Refinements in Finite Element Computations* (Edited by I. Babuška, O. C. Zienkiewicz, J. Gago and E. R. de A. Oliveira), pp. 119–129. Wiley, Chichester (1986).
36. O. C. Zienkiewicz, D. W. Kelly, J. Gago and I. Babuška, Hierarchical finite element approaches, error estimates and adaptive refinement. In *Mathematics of Finite Elements and Applications* (Edited by J. Whiteman), Vol. 4, pp. 313–346. Academic Press, London (1982).
37. R. J. Heck, J. Wei and J. R. Katzer, Mathematical modelling of monolithic catalysts, *AIChE J.* **22**, 477 (1976).
38. H. W. Braüer and F. Fetting, Stofftransport bei Wandreaktion im Einlaufgebiet eines Strömungsrohres, *Chem.-Ing.-Techn.* **38**, 30 (1966).
39. H. W. Bräuer and H. Schlüter, Konvektiver Stoffaustausch mit heterogenerer chemischer Reaktion, *Chem.-Ing.-Tech.* **37**, 1107 (1965).
40. G. Buzzi Ferraris, An optimization method for multivariable functions, *Working Party on Routine Computer Programs and the Use of Computers in Chemical Engineering*, Florence (1970).
41. C. W. Gear, The numerical integration of ordinary differential equations, *Math. Comput.* **21**, 146 (1967).
42. U. Grigull and H. Tratz, Thermischer Einlauf in ausgebildeter laminarer Rohrströmung, *Int. J. Heat Mass Transfer* **8**, 669 (1965).